Tikrit Journal of Engineering Sciences (2024); 31(1): 193-210
DOI: http://doi.org/10.25130/tjes.31.1.17

IRAQI Academic Scientific Journals

ISSN: 1813-162X (Print); 2312-7589 (Online)
Tikrit Journal of Engineering Sciences
available online at: http://www.tj-es.com

TJES
Tikrit Journal of Engineering Sciences

Design and Implementation of VSI for Solar Water Pump Control

Mohib A. Qasim, *Thamir H. Atyia* *
Electrical Engineering Department, Engineering College, Tikrit University, Tikrit, Iraq.

Keywords:
FOC; Induction Motor; MPPT; Perturb and Observe (P&O); Photo-Voltaic (PV); VSI Inverter.

Highlights:
- *Efficient and reliable system.*
- *Simplifies and reduces costs.*
- *Optimized power electronics and control.*

ARTICLE INFO
Article history:

Received	10 June	2023
Received in revised form	12 Aug.	2023
Accepted	04 Sep.	2023
Final Proofreading	23 Dec.	2023
Available online	06 Mar.	2024

Citation: Qasim MA, Atyia TH. **Design and Implementation of VSI for Solar Water Pump Control**. *Tikrit Journal of Engineering Sciences* 2024; **31**(1): 193-210.
http://doi.org/10.25130/tjes.31.1.17

*Corresponding author:

Thamir H. Atyia

Electrical Engineering Department, Engineering College, Tikrit University, Tikrit, Iraq.

Abstract: The hardware design, implementation, and digital control method for three-phase AC induction motors based on Field-Oriented Control is discussed in this work Solar-powered water pumping systems have become an practical option for remote irrigation and water supply as renewable energy sources obtain importance. This research enhances such systems performance and dependability by employing a Voltage Source Inverter. In order to optimize the energy transfer to the water pump, the recommended approach uses the Voltage Source Inverter capabilities to transform the variable DC output of the solar panels into a controlled AC supply. The research looks at the choice of power components, control algorithms, and modulation strategies while designing the Voltage Source Inverter. The most suitable modulation strategy is determined after an in-depth review of several different approaches to ensure greater pump performance. This research clarifies on how solar energy conversion and pump control work together to provide sustainable water management in off-grid areas. The research paper "Design and implementation of VSI for Solar Water Pump Control" demonstrates how solar water pumping systems can be optimized using power electronics and control. The project addresses efficiency difficulties and operational differences to create efficient and reliable solar-powered water delivery systems, which support environmental sustainability and rural development. Based on the power of the PV panel, the P&O MPPT method calculates the submersible pump speed. The sensorless speed control method eliminates the requirement for location or speed sensors. The Black Electro-Motives Force calculates speed by estimating the flux angle in the absence of mechanical speed sensors. This method reduces costs and simplifies the system simply by eliminating the requirement for expensive and complicated speed sensors. In order to determine steady-state and dynamic performance in varying insolation conditions, a prototype 5.5 KW inverter was constructed. In conclusion up, the research provided a thorough summary of the hardware and control aspects required for Field-Oriented Control in irrigation systems. The practical outcomes of this study have the potential to spur advancements in irrigation technology and the incorporation of renewable energy, resulting in substantial gains for agricultural productivity and environmental conservation.

تصميم وتنفيذ مصدر عاكس للجهد لمضخة مياة باستخدام الطاقة الشمسية كمصدر للتشغيل

محب احمد قاسم، ثامر حسن عطية

قسم الهندسة الكهربائية / كلية الهندسة / جامعة تكريت / تكريت – العراق.

الخلاصة

يقدم هذا العمل تصميم الأجهزة وتنفيذها وطريقة التحكم الرقمي على أساس تحكم توجيه الفيض المغناطيسي (FOC) للمحركات الحثية ثلاثية الاطوار. مع اكتساب مصادر الطاقة المتجددة مكانة بارزة، أصبحت أنظمة ضخ المياه التي تعمل بالطاقة الشمسية خيارا قابلا للتطبيق للري عن بعد وإمدادات المياه. باستخدام عاكس مصدر الفولتية، تعمل هذه الدراسة البحثية على تحسين أداء وموثوقية هذه الأنظمة. يستخدم النظام المقترح قدرات عاكس مصدر الفولتية لتحويل خرج التيار المستمر المتغير للألواح الشمسية إلى مصدر تيار متردد يتم التحكم فيه، مما يؤدي إلى تحسين نقل الطاقة إلى مضخة المياه. تبحث الدراسة في اعتبارات تصميم عاكس مصدر الفولتية، بما في ذلك اختيار مكونات الطاقة، خوارزميات التحكم، وتقنيات التشكيل. كذلك إجراء تحليل مقارن شامل للعديد من استراتيجيات التعديل لتحديد الطريقة الأنسب للحفاظ على الأداء الأمثل للمضخة. تسلط هذه الدراسة الضوء على الجمع بين تحويل الطاقة الشمسية والتحكم في المضخات، وتعزيز الإدارة المستدامة للمياه في الأماكن المعزولة عن شبكة القدرة الكهربائية. "تصميم وتنفيذ عاكس مصدر الفولتية للتحكم في مضخة المياه بالطاقة الشمسية" يوضح كيف يمكن لإلكترونيات القدرة والتحكم تحسين أنظمة ضخ المياه بالطاقة الشمسية. تتناول الدراسة صعوبات الكفاءة والاختلافات التشغيلية لبناء أنظمة فعالة وموثوقة لتوصيل المياه بالاستفادة من الطاقة الشمسية، وتعزيز الاستدامة البيئية والتنمية الريفية. تحدد خوارزمية P&O MPPT وسرعة المضخة الغاطسة على أساس القوة الدافعة الكهربائية (BEMF). ليست هناك حاجة إلى مستشعرات السرعة أو الموقع لتقنية التحكم في السرعة بدون مستشعر. بدون مستشعرات السرعة الميكانيكية، تقدر القوة الدافعة الكهربائية الخلفية زاوية التدفق المغناطيسي لتقدير السرعة. لاختبار الأداء المستقر والديناميكي في ظل حالات التشمس المختلفة، تم إنشاء نموذج أولي للعاكس بقدرة ٥,٥ كيلو وات. استخدم الاختبار الميداني مضخة غاطسة ثلاثية الطور ٣٠٠٠ دورة في الدقيقة، ٣٨٠ فولت/٥,٥ كيلو واط بعمق ٣٥ مترا في البئر. تم بناء مصفوفات الالواح الكهروضوئية على بعد ٣٥ كم شمال شرق مدينة الرمادي بالعراق، حيث لا توجد شبكة تجهيز كهرباء. تجهز كل لوحة كهروضوئية قدرة ٢١٠ وات على تتبع أقصى نقطة للقدرة (MPPT) 22.5 فولت وتيار ٩,٣٣ أمبير، وتحتوي المجموعة الكهروضوئية على ٧٥ لوحة.

الكلمات الدالة: تحكم توجيه الفيض المغناطيسي، المحرك التعريفي، الاضطراب والمراقبة (P&O)، الخلايا الكهروضوئية (PV)، عاكس VSI.

1.INTRODUCTION

Today's massive expansion in the global population and the ever-increasing demand for electricity have resulted in a worldwide issue reflected by the depletion of traditional energy sources and global warming. Using renewable energy sources is a partial solution to these issues [1,2]. Currently, solar energy is the preferred renewable source for driving water pumps in many countries [3,4]. In Iraq, diesel-operated water irrigation systems have been used for decades. However, the instability in the national grid, combined with the cost associated with diesel fuel for use in remote areas, has gradually lifted the popularity of PV-based irrigation systems. The AC Induction Motor (ACIM) is utilized in this project because it does not require permanent magnets, which would add to the cost, or brushes, which would degrade over time [5]. Therefore, ACIM is the most popular motor type in residential and industrial applications thanks to its durability, reliability, and simple construction, as the rotor is constructed simply from a steel cage. The ACIMs are operated at constant input frequency and voltage, but the motor can run at varied speeds if the frequency is variable. In this frequency variation, if the motor is not overloaded mechanically, the ACIM will rotate at speed proportional to the frequency input of the voltage source. A variation in the input voltage amplitude is necessary and must be proportional to the increase or decrease in frequency to keep the same current consumption magnitude. This method of keeping the same voltage over frequency ratio is called v/f or Volts-Hertz control [6]. The v/f control is simple to implement as it has no complex control loops and does not require pre-knowledge of the motor's electrical parameters. As a result, it is widely used in "cheap" AC motor drives. However, this control method lacks the ability to control the flux and current of the motor, and the speed control requires mechanical speed sensors. Since the speed, sensors are impractical to install in some environments or already installed systems [7]. In high-performance motorized systems, controlling current, torque, and flux is challenging in ACIMs due to the complexity of modeling mathematically and oscillation in electrical parameters with temperature variations, and it behaves nonlinearly at saturation [8,9]. As this is the case with ACIMs, higher-performance algorithms are often used to overcome the issues presented in the classical v/f control method. One of the alternative algorithms is vector control, which is a rather complicated algorithm, and hence, it requires a powerful MicroController Unit (MCU) to execute. During the last three decades, electrical motor drives based on field control have witnessed a rapid boost due to the introduction of microcontrollers [10]. Embedded device technology improvements have led to efficient and effective control of AC motor drives, and more sophisticated high-performance control structures have been introduced. The control structures of such drives can accurately control not only the DC quantities, but also the AC voltages and currents by the vector control techniques. The present paper briefly illustrates the implementation of the AC motors' most efficient vector control structure: The Field-

Oriented Control (FOC) for PV-powered ACIMs. The FOC control topology relies on three points:

- Voltages and currents space vectors of the ACIM
- System three-phase time- and speed-dependent transformations into two-coordinate quantities (time-invariant system) using forward and reverse Clarke and Park transformations.
- Generation of Space-Vector Pulse Width Modulation (SVPWM) patterns to control the three-phase inverter power stage [11].

In the FOC algorithm, the control of ACIM is done by utilizing every advantage in DC motors control by transforming three-phase AC quantities into rotating reference frame (d-q coordinates), allowing a very precise transient and steady-state control, resulting in a high performance as far as the DC-AC conversion efficiency and controller response time are concerned [12]. Several studies have focused on designing and implementing a Voltage Source Inverter (VSI) for solar water pump control. High-performance electrical drive systems use the FOC control method, in particular, for controlling AC induction motors. To control the essential load voltage components [13], FOC uses pulse width modulation in conjunction with linear controllers. The FOC method separately controls the torque and rotor flux using a current space vector consisting of two orthogonal components [14]. The non-linear structure of the induction motor drive is made simpler and more precise speed control is made possible by this control separation [15]. A solar photovoltaic-powered brushless DC motor drive for water pumping was demonstrated by Kumar and Singh [16]. The motor speed was controlled by adjusting the VSI DC bus voltage. They removed the requirement for voltage sensors on the VSI's DC bus and current sensors on the BLDC motor. In a separate research, Kumar and Singh [17] powered a BLDC motor in a solar PV array-powered water pumping system using a zeta converter and three-phase VSI. To ensure that the SPV array works at its maximum power point, they designed an incremental conductance maximum power point tracking method. The system's initial, dynamic, and steady-state behaviors were simulated and researched using MATLAB/Simulink software. For water pumping applications, Narendra et al [18]. proposed a sensorless speed control system for an introduction motor that uses a single-stage SPV fed reduced switching inverter. In order to reduce switching losses and expenses, they tried to decrease the number of switches in the system. They used an adapted incremental conductance technique to reach the reference voltage and a speed estimator to design a sensorless speed control. The IM was controlled via Direct Vector Control. Hassan [19] examined a solar-powered water extraction system's design and simulation. The analysis focused on the system's optimal operating point and efficacy. The research clarified the effectiveness of solar pumping systems and the choice of appropriate designs. A solar photovoltaic off-grid water pumping system design based on an improved fractional open circuit voltage MPPT approach was proposed by Hmidet et al [20]. They created a fuzzy precompensated hybrid proportional-integral controller for a permanent magnet motor-driven solar water pumping system in order to overcome the shortcomings of conventional controllers. To enhance the performance of the PV water pumping system, they also proposed indirect field-oriented control for an IM lacking an energy storage system. Lalithasymala and Ravi Kishore [21] compared VSI and current source inverter (CSI) based solar photovoltaic source-fed BLDC motor drives with a boost converter for a water pumping system. The authors emphasized the benefits of using a CSI instead of a VSI, such as reduced converter switch tension and cost. Singh and Kumar [22] focused on a water pumping system powered by solar photovoltaic arrays and managed by buck-boost converters. They aimed for the best possible SPV array performance as well as the natural start of a permanent-magnet BLDC motor. They avoided the use current sensors of the BLDC motor by adjusting the VSI's DC-link voltage. Sinaga [23] emphasized how important it is to have an efficient and successful design for water pump control systems. They suggested a control system that takes into account groundwater and water reactions, as well as the connections between supply and demand for water. A second control system, proposed by Samikannu et al. [24], controlled the connection time between solar modules, batteries, and water pumps by using fuzzy management methods. For the intelligent regulation of an induction motor operating in marine water pumping applications, they created a modular multilevel inverter. The proposed eleven-level inverter made it possible to regulate the solar photovoltaic-powered IM drive. A battery-assisted solar water pumping device with several off-grid uses was presented by Vamja and Mulla [25]. They created an advanced control system that improved the use of the solar photovoltaic source and managed battery power through the DC-DC converter. During power supply operations, the domestic electrical capacity was connected to the system, and the VSI was used as a variable frequency motor drive for pumping operations. Several research works have looked into the implementation and design of VSIs for solar water pump control. This research compared VSI and CSI, applied intelligent control

methods, removed current and voltage sensors, and employed the methods of MPPT for sensorless speed control. These studies provide valuable insights for the design of efficient and dependable solar water circulation systems. An incremental conductance (INC) MPPT algorithm controls the zeta converter so that the SPV array always operates at its MPP, and the starting current of the BLDC motor is reduced. For the electronic commutation of the BLDC motor, a three-phase Voltage Source Inverter (VSI) employs fundamental frequency switching. MATLAB/Simulink simulation results are examined to illustrate the commencing, dynamics, and steady-state behavior of the proposed water pumping system subject to random variation in solar irradiance [26]. The main contribution of this paper is that a voltage source inverter (VSI) transforms DC solar power into AC water pump power through control systems, modulation algorithms, and VSI topologies. The work may develop a solar water pumping system control approach. MPPT algorithms can optimize solar panel output, water pump speed, and efficiency based on solar energy. Hardware implementation: solar panels, VCI, actuator, sensors, and plug-ins are specified by the project. Components, specs, and connections are listed here. Programming controls algorithms. The project may target real-world control strategy software architecture, programming languages, and tools. Experimental data and performance assessments will support early contributions. This section should show the efficiency benefits of the suggested control algorithms, comparisons with ordinary water pumping systems, and system performance under varied solar circumstances. Solar water pumps may save electricity and the environment. Solar energy systems use less energy and emit less carbon. Technical efforts address design and implementation challenges, suggest research topics, and discuss the system's flexibility, scalability, and versatility. The paper has been divided into nine sections. The first section is an introduction. The second section expounds on the Problem Statement in the first section. In the third section, the notion of field-oriented control was discussed. A description of the FOC Control Structure is in section four. The MPPT Algorithm and the Simulation Results are discussed in the fifth and sixth sections, respectively. The seventh section deals with validating the hardware. Results from the field are shown in the eighth section. Finally, the conclusions are presented in the ninth section.

2.PROBLEM STATEMENT

Solar water pumps are popular for their eco-friendliness and low cost. Solar pumps pump water for agricultural, home, and commercial uses. Voltage Source Inverters (VSI) transform solar panel DC electricity into AC voltage to run solar water pumps. By making use of a Voltage Source Inverter (VSI) control method it can generate a dependable solar water pump. The method should productively transform solar panel DC electricity into AC power for the motor. The objectives are maximum water supply, every efficiency and pump life.

Keys of problem statement:

(1) Efficient power conversation: Progress procedures and administer techniques to productivity transform solar power panel DC power into balanced and restrained AC power for running the pump motor.

(2) MPPT: Use a reliable MPPT method to observe the solar panels maximum power point to maintain the system operating adequately disregarding the changing states of sunshine.

(3) Voltage and Frequency Control: present control mechanisms that keep VSI output voltage and frequency even when solar conditions vary to assure pump accuracy and solidity.

(4) Dynamic Load Management: organize a management system to handle changeable water requirements and adjust the pump rate to suit load demands while optimum energy use.

(5) Safeguard the VSI and pump motor from excessive voltage, overcurrent, and other faults.

(6) Scalability: Develop a convenient interface that allows uses observes system performance, adjust pump settings and receive warnings.

(7) Scalability: Design the system to handle variable pump sizes and water demands without changing the control algorithm.

3.FIELD ORIENTED CONTROL ALGORITHM

Early developed control structures, such as the v/f control structure, seriously limit the system's performance. A more sophisticated algorithm was applied to the ACIM machine implement better performance control. With the powerful math-processing power offered by modern MCUs, advanced control algorithms and strategies that use mathematical transformations and equations can be implemented. As a result, magnetization functions ACIMs and torque generation can be decoupled and controlled. This decoupling in torque and control of magnetization (flux control) is called Field- or Flux-Oriented Control, simply FOC [27]. In the traditional v/f control method, the ACIM drive (inverter) controls only the motor's three-phase voltage amplitude and frequency. In contrast, in the FOC control scheme, the frequency, phase, and amplitude of the ACIM drive voltage are controlled. The key to this algorithm is to

produce a three-phase phasor voltage to control the three-phase current of the ACIM stator that, in turn, controls the flux vector of the rotor. As a result, the rotor current phasor can be controlled similarly to the brushed DC motor speed control, which means that both torque and flux can be controlled separately using this approach. Two major concepts of the FOC control algorithm are described as follows:

A_ Space-Vector Projection and Definition

Analyzing a complex space vector can simplify three-phase currents, voltages, and fluxes in ACIM machines. Assuming I_a, I_b, and I_c are the instantaneous AC currents of the ACIM stator, the complex space vector in the stator can be defined as:

$$\vec{I_s} = I_a + \alpha I_b + \alpha^2 I_c \quad \textbf{(1)}$$

where $\propto = e^{j\frac{2}{3}\pi}$ and $\propto^2 = e^{j\frac{4}{3}\pi}$ are the representations for spatial operators, as shown in Fig.1.

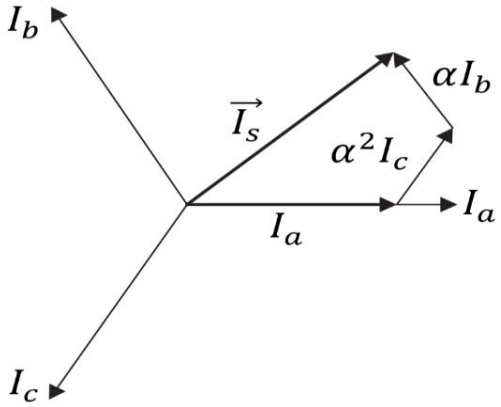

Fig. 1 Space Vector of ACIM Stator Current with its Three Components (I_a, I_b, **and** I_c).

This current space vector represents the sinusoidal three-phase system and should be transformed into a time-invariant (rotating frame) coordinate system with two components. The transformation can be evaluated using the following two steps:

- Clarke Transformation (abc → αβ) that outputs a two-coordinates of time-variant system.
- Park Transformation (αβ → dq) that outputs a two-coordinates of time-invariant system.
- *Clarke Transformation (abc → αβ Projection)*

Only two orthogonal time-variant axes, i.e., α and β, can describe three-phase quantities, assuming the phase is matched with α. Fig. 2 shows the vector diagram for Clarke transformation.

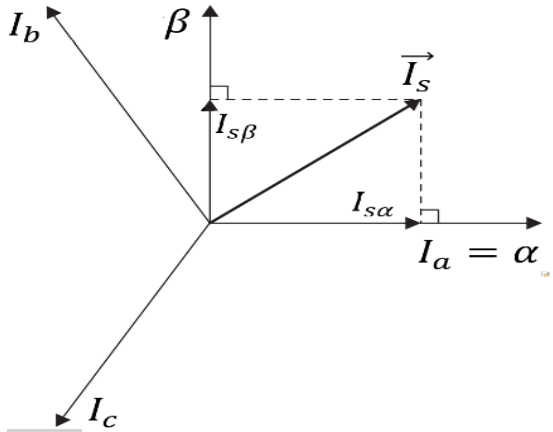

Fig. 2 Space Vector of Stator Current with its Two Components (α, β) in the Stationary Reference Frame.

This projection converts the three-phase quantities into two orthogonal time- and speed-variant systems that can be described in Eqs. (2) and (3):

$$I_{s\alpha} = I_a \quad \textbf{(2)}$$

$$I_{s\beta} = \frac{1}{\sqrt{3}}(I_a + 2I_b) \quad \textbf{(3)}$$

B_Park Transformation (αβ → dq Projection)

Park transformation is the core transformation in FOC control and the most important one. This transformation projects the two stationary reference frame orthogonal quantities (α, β) into two rotating reference frame quantities (d, q), as shown in Fig. 3.

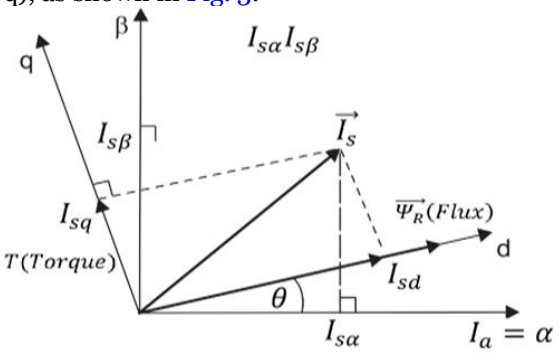

Fig. 3 Space Vector of ACIM Stator Current with its Stationary Components (α, β) and Rotating Components (d, q).

where θ and $\vec{\Psi_R}$ are flux position angle and flux vector, respectively, and the torque (I_{sq}) and flux (I_{sd}) components for the current vector can be obtained using Eqs. (4) and (5):

$$I_{sd} = I_{s\alpha}\cos(\theta) + I_{s\beta}\sin(\theta) \quad \textbf{(4)}$$

$$I_{sq} = I_{s\beta}\cos(\theta) - I_{s\alpha}\sin(\theta) \quad \textbf{(5)}$$

According to the equations above, these two components are influenced by the stationary current vector components (α, β) and the rotor flux position angle (θ). The (d, q) components of the ACIM motor flux angle are produced by

this translation. Since the d and q components of a balanced system are time-invariant, two DC components represent the three-phase currents in the ACIM. Classic Proportional-Integral (PI) controllers can control the flux (d-component) and torque (q-component) separately due to their DC nature.

4.METHODOLOGY Of FOC CONTROL STRUCTURE

As illustrated in Fig. 4, current sensors detect ACIM phase currents first. Physically measuring just two-phase currents optimizes cost. The three-phase motor's phase currents are equal; hence Ic = -Ia - Ib gives the third phase current. Clark transformation block transforms three-phase currents into stationary reference frame components (α, β). The Park transformation block produces the rotating reference frame from (α, β) and (d, q) DC values for flux and torque. Isq and Isd are compared to reference torque and flux at these positions. At this level, torque and flux may be regulated separately. This approach controls three-phase synchronous and asynchronous (induction motors) machines by altering the flux reference (d-component) and determining the flux position angle.

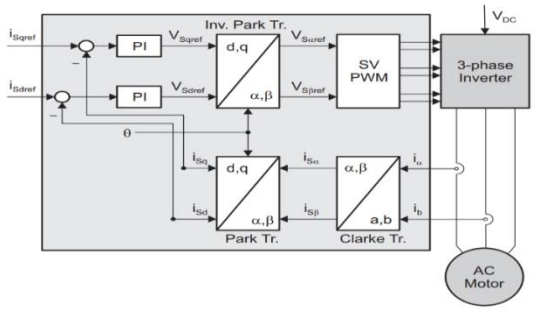

Fig. 4 Basic Structure of FOC for ACIM.

For ACIM, the rotor needs flux for the machine to spin, and therefore, flux generation is required by setting a proper value to I_{sdref} in the FOC control structure. This concept is considered the most valuable advantage of FOC control since it enables interchange between synchronous and induction machine drives. The torque reference, I_{sqref} input, could be the output from the speed regulator when the FOC is used as a speed controller. In current regulators, the difference (error) between reference values and actual measured values for torque and flux (I_{sd} and I_{sq} signals) are input to PI controller blocks for rotating current components regulation. The output from current regulators' PI blocks is considered the reference values (V_{sdref}, V_{sqref}) for the voltage components that should be output to the ACIM by the VSI inverter. These two reference signals are then fed to the inverse Park transformation block to obtain the reference stationary orthogonal frame values ($V_{s\alpha ref}$, $V_{s\beta ref}$). These two signals are then fed to the SVPWM, which inevitably can create and evaluate control systems structures and PI controllers, which may be modeled in Simulink with the use of the Simulink Control Create tool. Integrating PI auto-tuning into the embedded software will allow the PI gains to be automatically computed in real-time. The SVPWM use in designing and implementing a VSI for solar water pump control provides several benefits, including increasing efficiency, reducing harmonic distortion, improving torque and speed control, decreasing switching losses, enhancing thermal management, and decreasing acoustic pollution. These advantages contribute to an overall more reliable and efficient system, making SVPWM a popular option for motor control in applications involving solar water extraction. The SVPWM generator outputs six Pulse Width Modulated (PWM) signals that drive the inverter power switches. In Fig. 4, the rotor flux position, θ, is required in both forward and reverse Park transformation blocks. In the sensored FOC control systems, this angle is measured using mechanical or hall-effect sensors that measure the speed and angle in real-time. Meanwhile, in the senseless FOC control, the flux position is estimated using the Back Electro-Motive Force (BEMF) and mathematical equations and is discussed in the following section. The BEMF is first calculated from the flux and speed estimator inputs shown in Fig. 5. The speed estimation in a motor can be achieved by estimating the flux angle relying on the back electro-motive force (BEMF) [18].

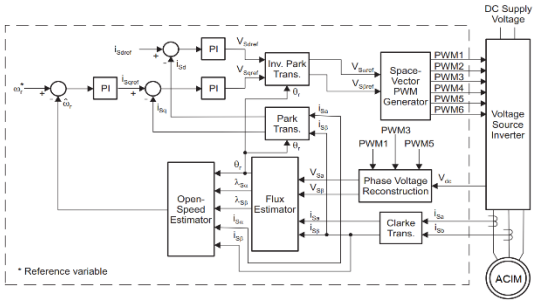

Fig. 5 Basic Structure of FOC for ACIM.

The orthogonal stationary components of the BEMF (Eα and Eβ) are calculated by Eqs. (6) and (7):

$$E_\alpha = V_{s\alpha} - R_s I_\beta - \delta L_s \frac{dI_\alpha}{dt} \quad \textbf{(6)}$$

$$E_\beta = V_{s\beta} - R_s I_\beta - \delta L_s \frac{dI_\beta}{dt} \quad \textbf{(7)}$$

where R_s, L_s, and δ are stator resistance, stator inductance, and leakage coefficient found from the motor manufacturer datasheet. The rotating reference frame values of the BEMF (E_d and E_q) are computed using Eqs. (8) and (9):

$$E_d = E_\alpha \cos(\theta_r) + E_\beta \sin(\theta_r) \quad \textbf{(8)}$$

$$E_q = E_\beta \cos(\theta_r) - E_\alpha \sin(\theta_r) \quad \textbf{(9)}$$

where θr is the estimated rotor angle. Now, since the BEMF is directly proportional to the rotor flux variation, Ψ_{mR} , Eq. (10):

$$\vec{E} = \frac{1}{1+\delta_R}\frac{d}{dt}(\Psi_{mR}) \quad (10)$$

Splitting d and q components of BEMF:

$$E_d = \frac{1}{1+\delta_R}\frac{d}{dt}(\Psi_{mR}) \to 0 \quad (11)$$

$$E_q = \frac{1}{1+\delta_R}\Psi_{mR}\,\omega_{mR} \quad (12)$$

where δ_R and ω_{mR} are the rotor leakage coefficient and rotor estimated speed, respectively.
Hence, the rotor speed can be put as in Eq. (12):

$$\omega_{mR} = \frac{1+\delta_R}{\Psi_{mR}}E_q \quad (13)$$

Equations (10) and (11) were obtained, considering constant rotor flux. However, an estimation error is produced if the d-component of the BEMF, E_d is not zero. This error is approximately equal to the E_d term and should be removed manually by subtracting or adding the nonzero value (depending on the error sign). Therefore, the rotor estimated speed is written as:

$$\omega_{mR} = \frac{1+\delta_R}{\Psi_{mR}}\{E_q - sign(E_q)E_d\} \quad (14)$$

The rotor estimated angle is now can be calculated by integrating the estimated speed or:

$$\theta_r = \int \omega_{mR}\,dt \quad (15)$$

Fig. 6 shows the speed estimation block diagram.

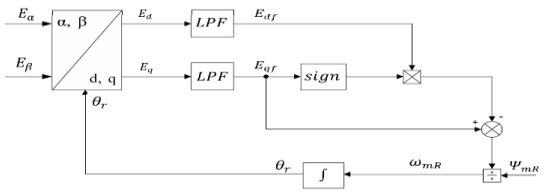

Fig. 6 Estimated Rotor Angle and Speed by Assuming Constant Flux.

5.MPPT ALGORITHM

The MPPT algorithm extracts the maximum power from the PV array by adjusting the reference speed of the FOC speed control system [28]. The algorithm is based on the famous Perturb and Observe (P&O) [29]. The algorithm is started by reading the voltage and current of the PV array (input DC voltage of the VSI inverter). It then calculates the PV array power from voltage and current measurements and subtracts it from the previous power read to calculate the power change variable, ΔP, as denoted by the block diagram in Fig. 7. If a positive ΔP is observed, it means that an increase in power drawn from PV array is detected, and the last decision of increasing or decreasing the reference speed of the water pump was right.

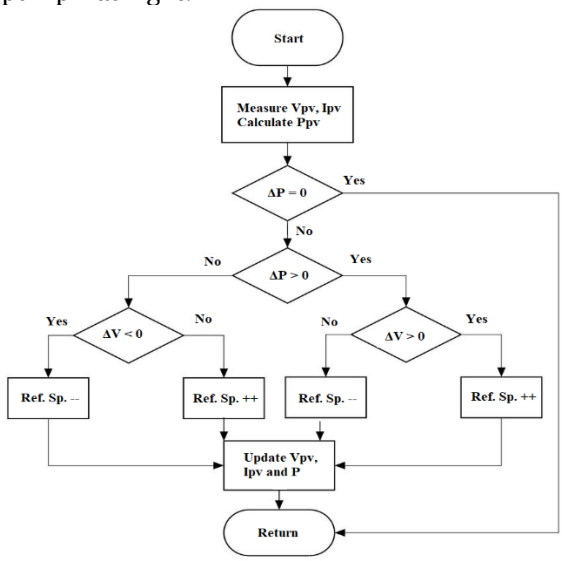

Fig. 7 P&O MPPT Algorithm for Maximum PV Power Extraction.

In this case, the controller will continue to increase or decrease the speed as the last time to attempt further increase in the PV array power. When a negative ΔP occurs, the last decision to change the speed reference was wrong, and it must be reversed compared to the previous MPPT execution cycle. The increase in ACIM speed reference means it will draw more current as the motor's power is directly dependent on speed and output torque. Therefore, the speed setting of the motor will have a reverse impact on the PV array voltage. The MPPT controller will, therefore, use the PV voltage change, ΔV, to determine whether to increase or decrease the desired speed that gives the maximum power from the PV array.

6.SIMULATION RESULTS

The system simulation uses MATLAB to verify the design prior to hardware modeling. The simulation block diagram is shown in Fig. 8. A nonlinear equivalent circuit model of an induction motor is considered to determine the values of the reference flux linkage. This method generates a lookup table by performing an offline calculation to identify the reference flux linkage using the nonlinear equivalent circuit characteristics. In MATLAB/Simulink ACIM systems with SVPWM and motion control, a flux versus speed lookup table is utilized to optimize the motor's efficiency, achieve accurate control under varying conditions, handle nonlinearities, facilitate sensorless control, reduce computational complexity, adapt to motor variations, and guarantee smooth transitions and dynamic responses. Fig. 9 to Fig. 11. Simulations in MATLAB accurately predicted output speed with a maximum variance of 0.87 percent. The used control method may have performed admirably in simulation. Prior to hardware

implementation, the control method must be validated. Frequently, the design of control systems contrasts actual and predicted speed under various torque conditions (Fig. 9). It demonstrates how the management algorithm operates under various operational and demand conditions. The small divergence of this model suggests that it accurately anticipates motor behavior. As previously stated, increasing the ACIM speed reference will necessitate an increase in motor current because motor power influences speed and torque directly. More electricity is required to generate torque at higher velocities. Fig. 10 shows that for voltage source inverters using SVPWM methods, the duty ratio is a significant operating parameter. The duty ratio must be carefully regulated in conjunction with the switching strategy when using reduced switching SVPWM to achieve the appropriate reduction in switching frequency while maintaining the necessary output voltage levels and system performance. SVM is a typical approach for controlling the output voltage of a three-phase inverter to power AC motors. It improves the output waveform and harmonics. The "reduced switching SVPWM" shown in Fig.11 is a modified SVM that reduces switching losses. Duty Ratio and Fluctuation Factor: The duty ratio of PWM control determines the pulse breadth of the motor to produce the required output voltage. The duty ratio profile of the motor may indicate its evolution. The discussion above shows that the Space Vector PWM is superior to sinusoidal PWM in many aspects: 1) The Modulation Index is higher for SVPWM than SPWM. 2) The output voltage is about 15% higher in SVPWM than in SPWM. 3) The current and torque harmonics are reduced but not eliminated.

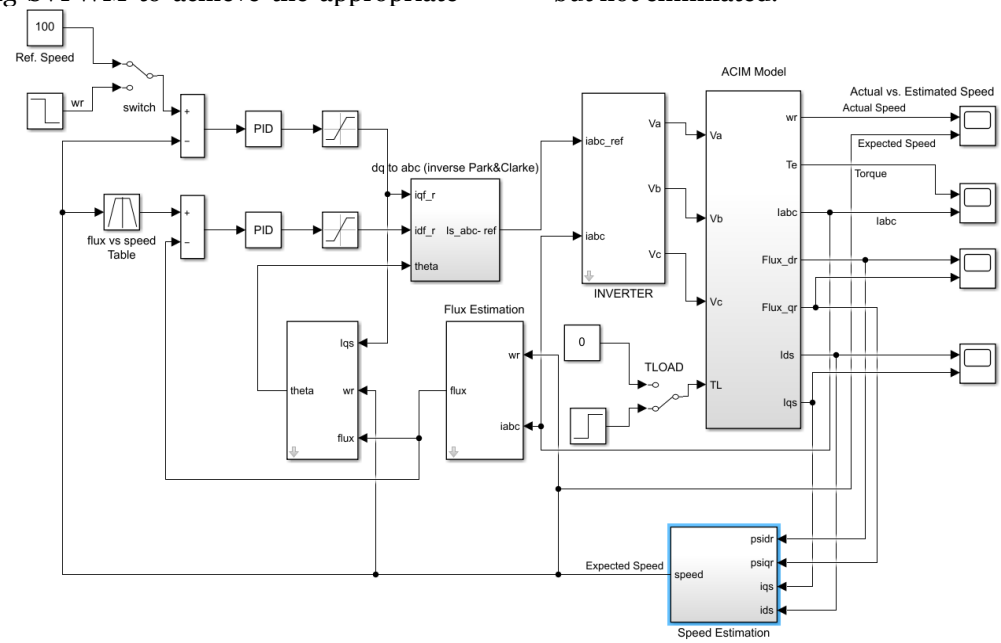

Fig. 8 System Simulation Block Diagram Using MATLAB.

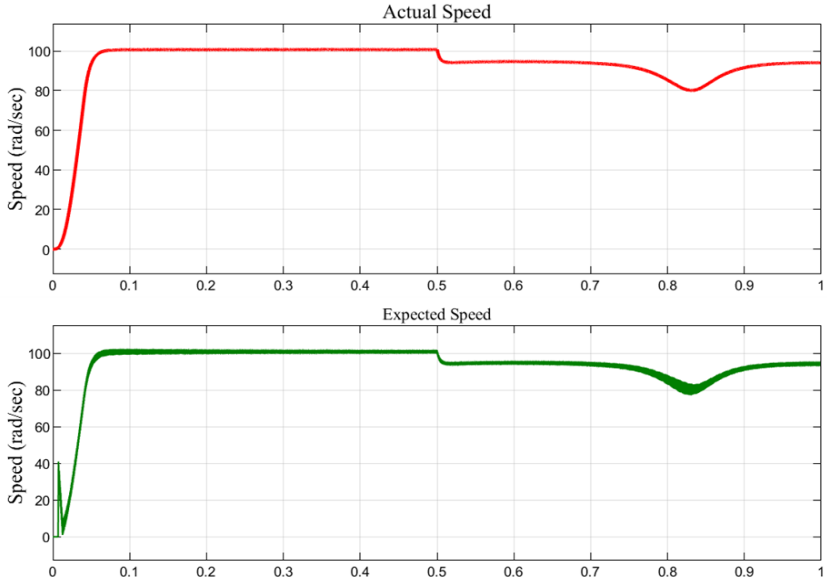

Fig. 9 Actual (Top) vs. Estimated (Bottom) Speed for the System Simulation.

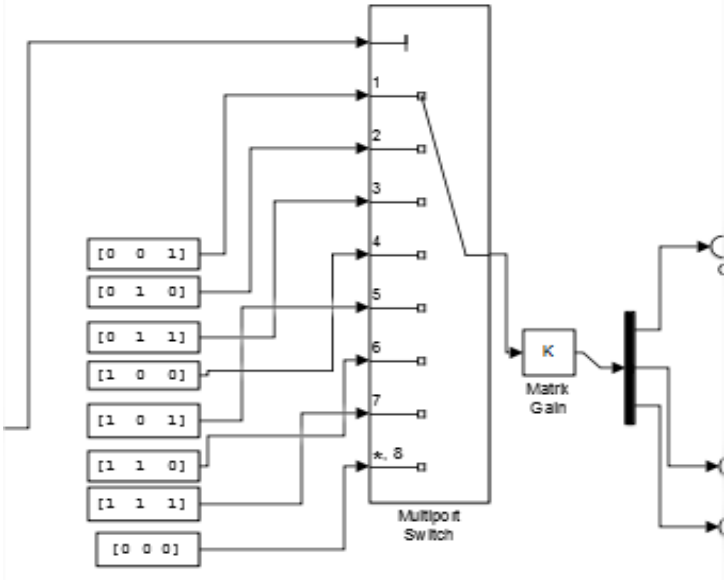

(a)

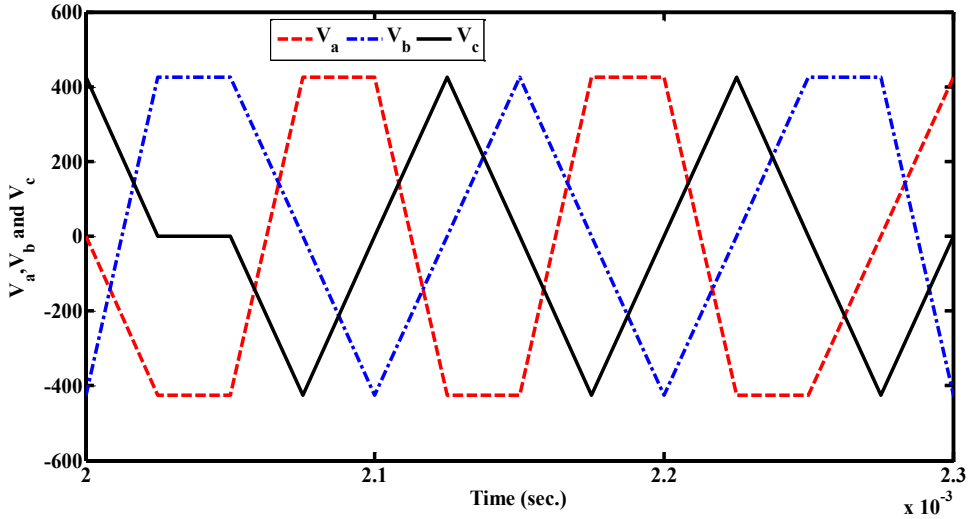

(b)

Fig.10 (a) Space Vector Modulation Simulink model, (b) Profile of Duty Ratio with Reduced Switching SVPWM.

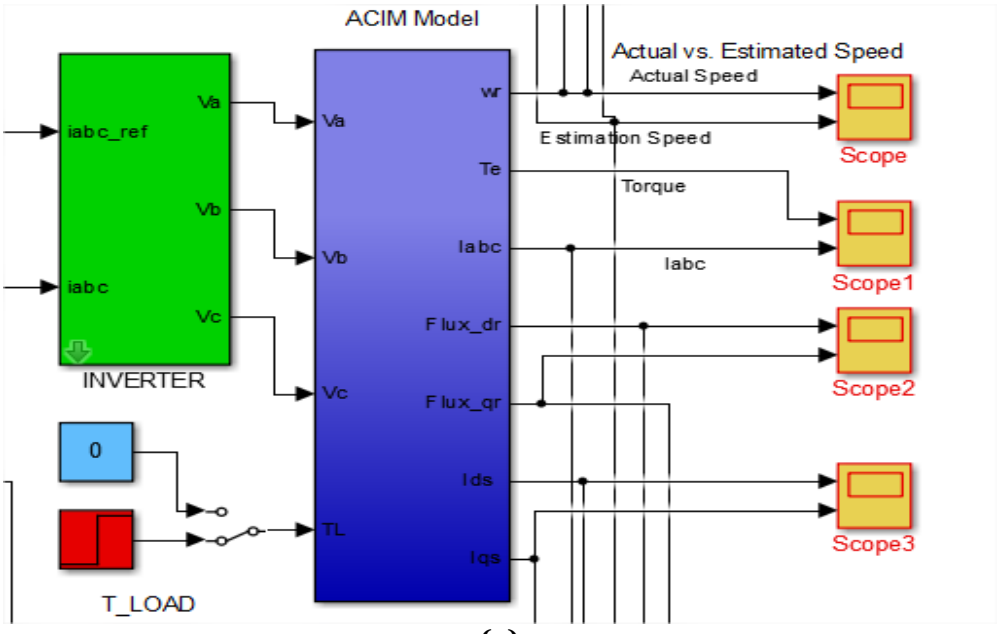

(a)

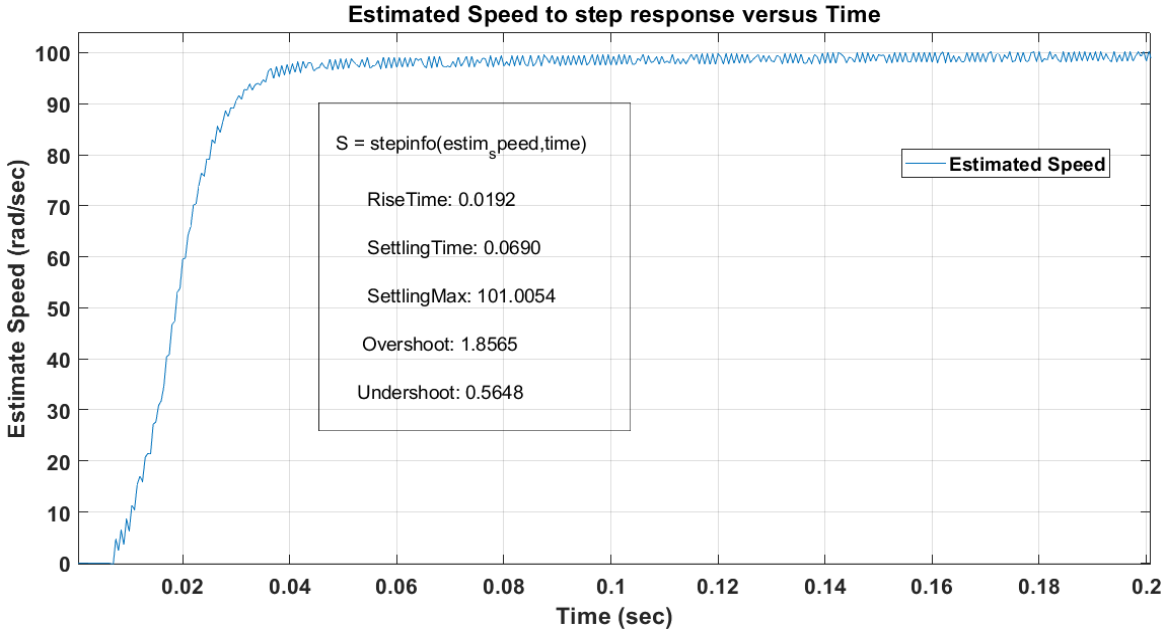

(b)

Fig. 11 Estimated Speed to Step Response.

Simulation results of the proposed system based on the Matlab/Simulink model are analyzed and compared with those obtained from the practical results. Fig. 12 shows the current waveform of phase A versus the estimated angle. Fig. 13 depicts the motor current's stationary reference frame components (α, β). The motor speed is then suddenly changed from 2500 to 2400 rpm to mimic a falling step change for the speed controller behavior testing of good tracking speed changes, as shown in Fig. 14. Part of the simulation results obtained by running the Matlab/Simulink model of the proposed system is presented in Fig. 15, showing the three-phase voltages (Va, Vb, Vc). The three-phase currents (Ia, Ib, and Ic) are displayed in Fig. 16, and the electromagnetic torque is depicted in Fig. 17.

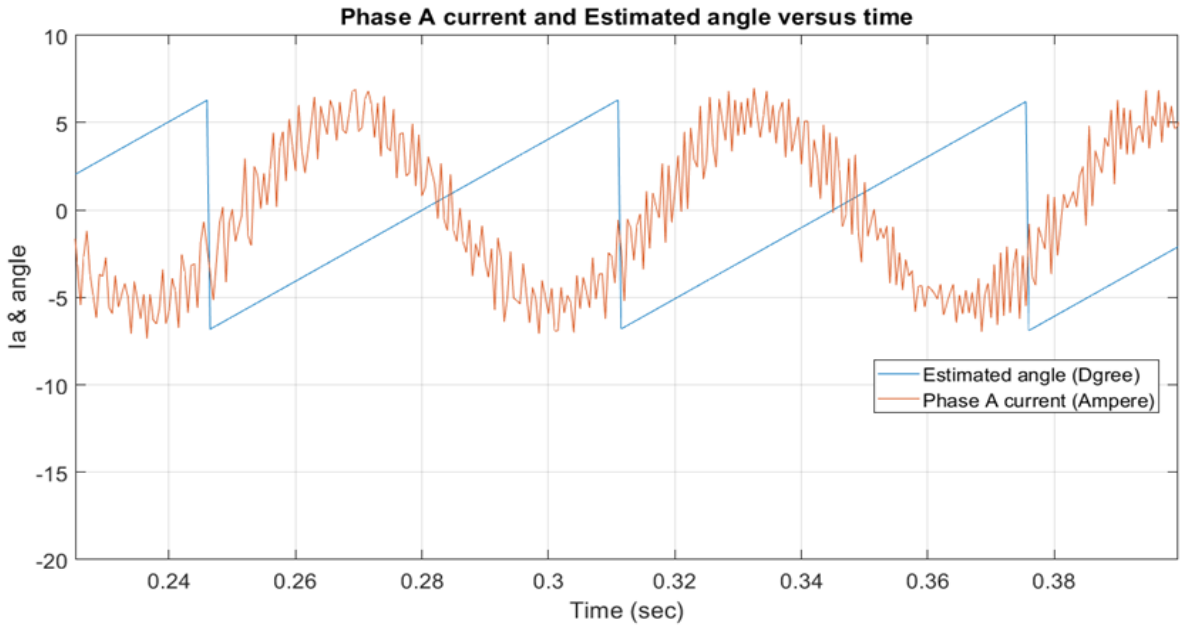

Fig.12 Phase A Current (Brown) and Estimated Angle (Blue) Versus Time at 2500 rpm.

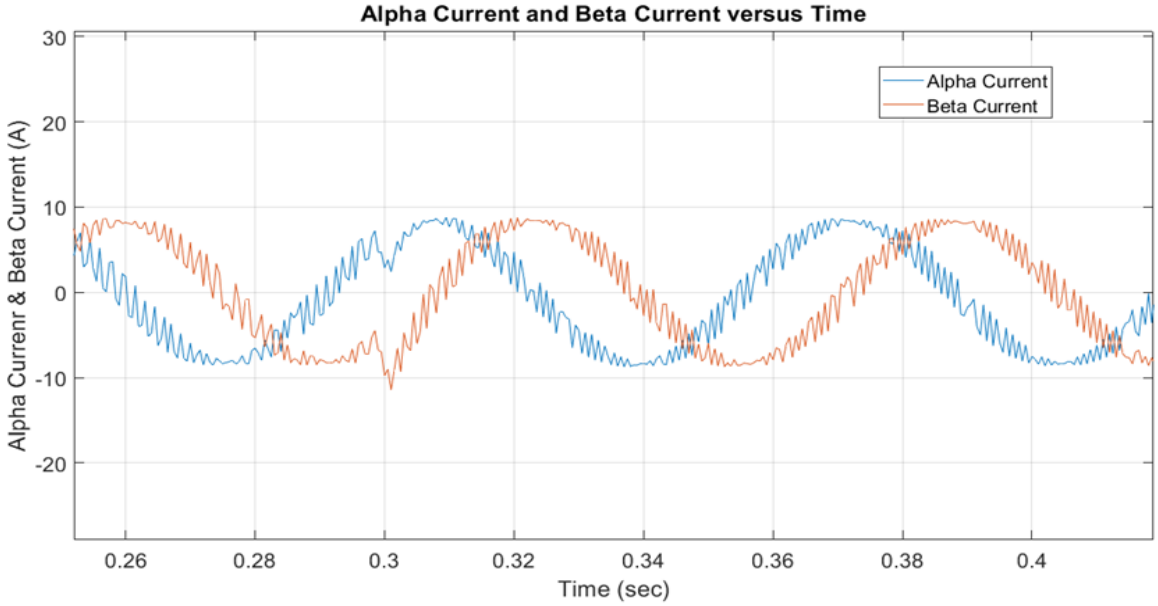

Fig. 13 (α, β) Components of Motor Current.

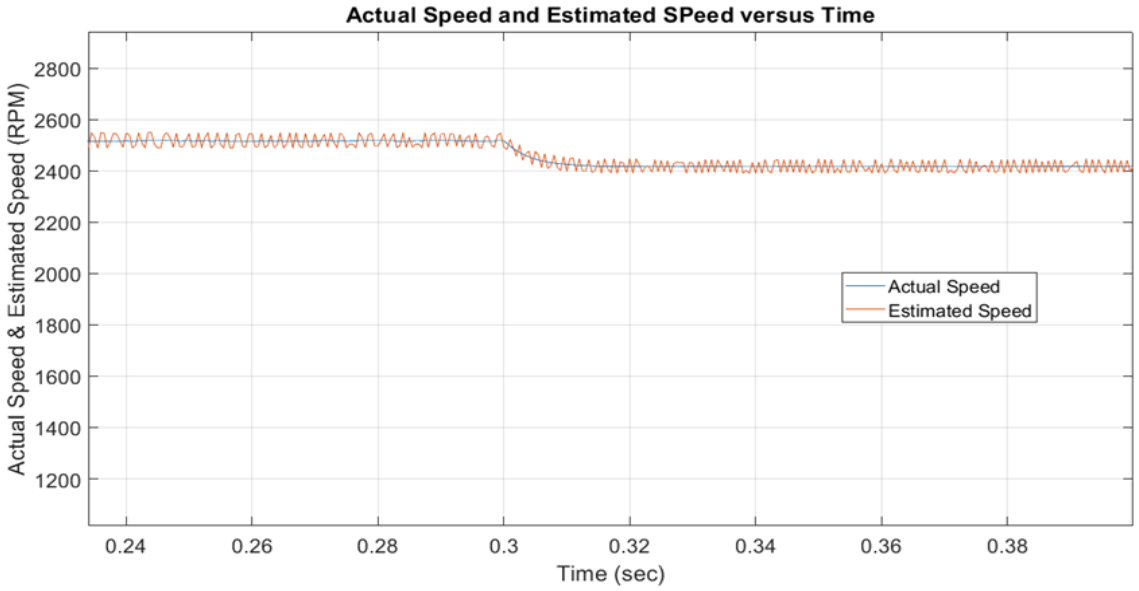

Fig. 14 Actual (Blue) and Estimated (Brown) Speed Versus Time for the Implemented System.

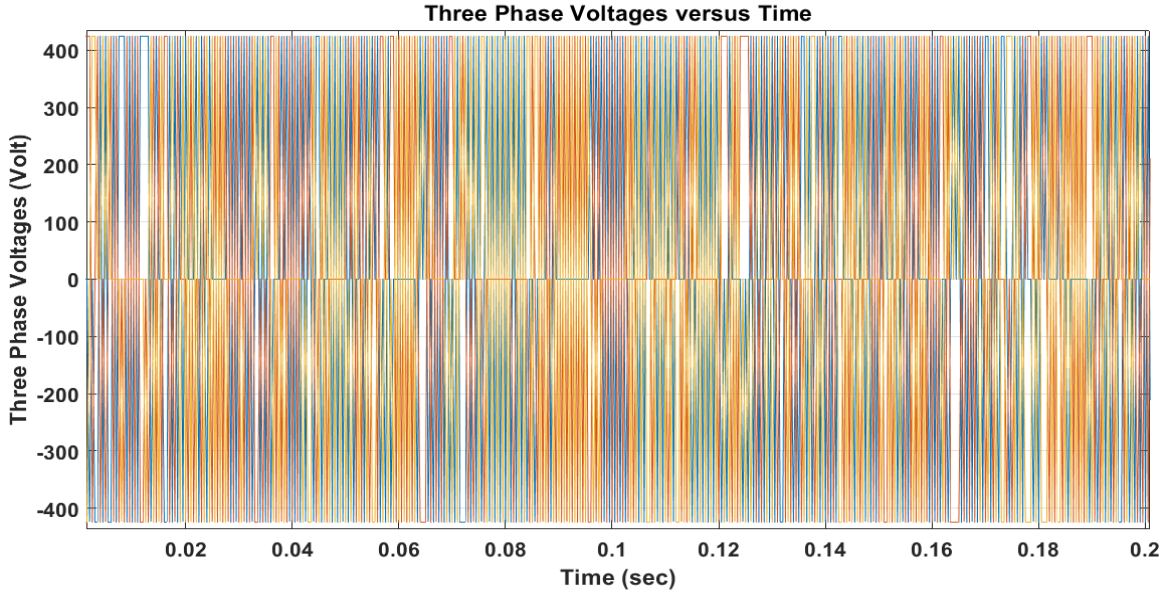

Fig. 15 Three Phase Voltages (Va, Vb, and Vc).

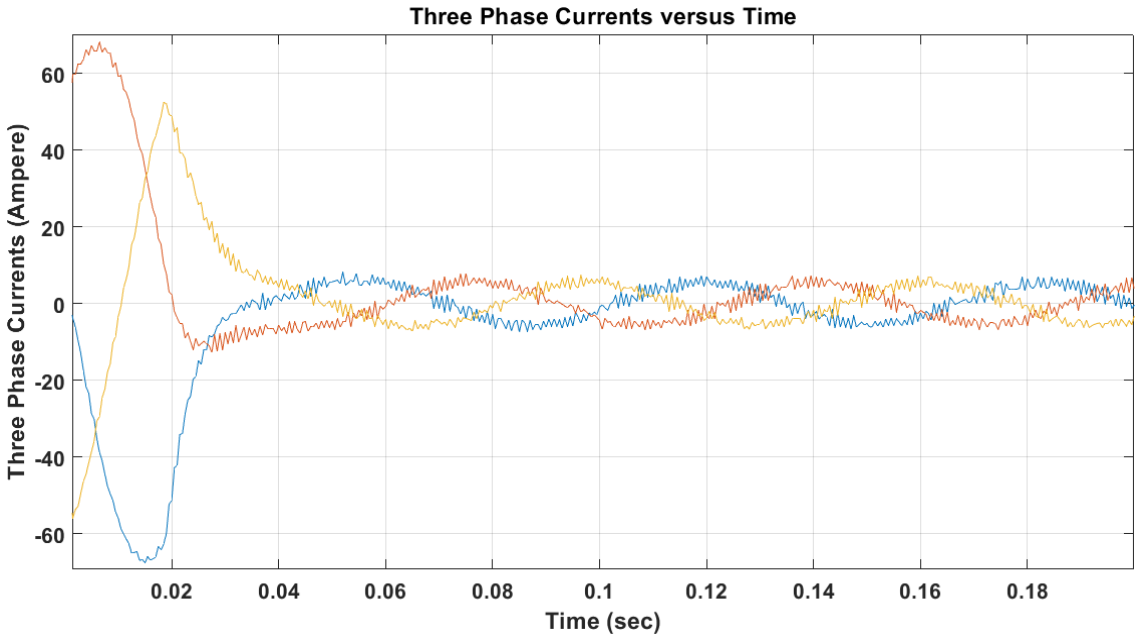

Fig. 16 Three Phase Currents (Ia, Ib, and Ic).

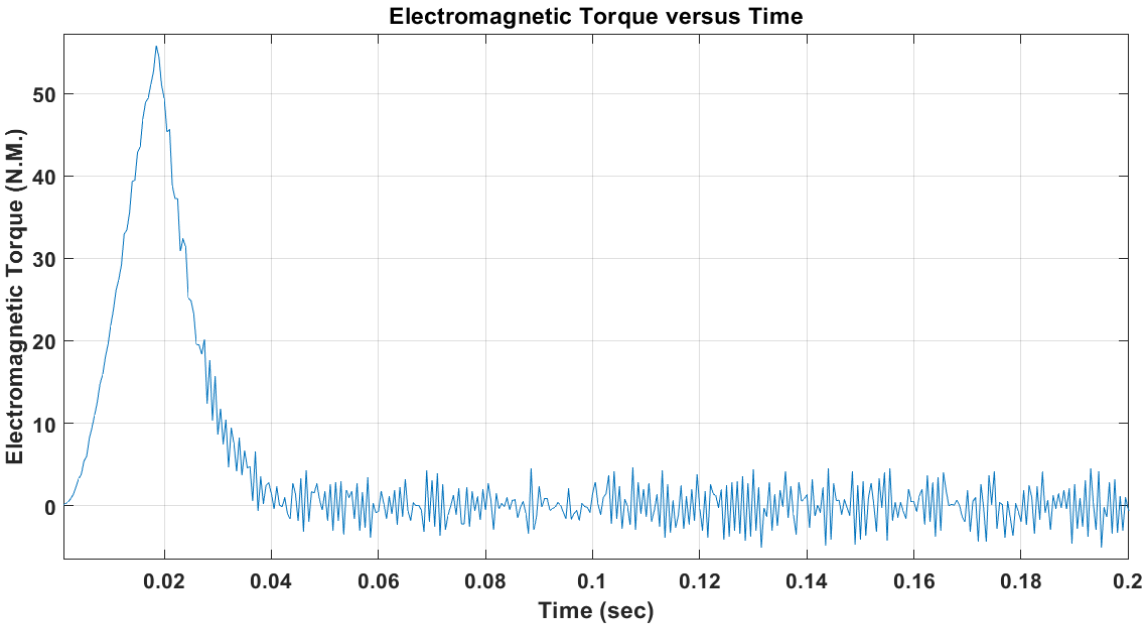

Fig. 17 Electromagnetic Torque to Step Response.

7.HARDWARE VALIDATION

The designed system has been verified in reality by designing a 5.5 kW VSI inverter board prototype based on an IGBT power switch (Infineon IKW40N120H3). The designed inverter controller is a Texas Instruments F28054FPNQ C2000 microcontroller. The board has an isolated Controller Area Network (CAN) to communicate with other hosts for control and data acquisition. The IGBT driver topology is a non-isolated boot-strap driver IC, FAN73912. The current sensing uses three shunt resistors based topology with TLV9064 quad op-amp for current signal conditioning. The developed inverter is shown in Fig. 18. The system was tested in the field where it used to operate a 3000 rpm, 380V/5.5 kW three-phase submersible pump 35 m deep in the well. The PV array was installed in a remote area with no utility grid (35 km northeast of Ramadi city, Iraq). The PV array was constructed from three parallel 25 PV panel series (75 panels in total); each PV panel is a 210W with Maximum Power Point (MPP) voltage and current of 22.5V and 9.33A, respectively. The lab-in-the-field configuration is shown in Fig. 19. The designed system has been installed to irrigate 2.5 Hectares (25,000 m2) of wheat fields in the western desert of Iraq, as shown in Fig. 20.

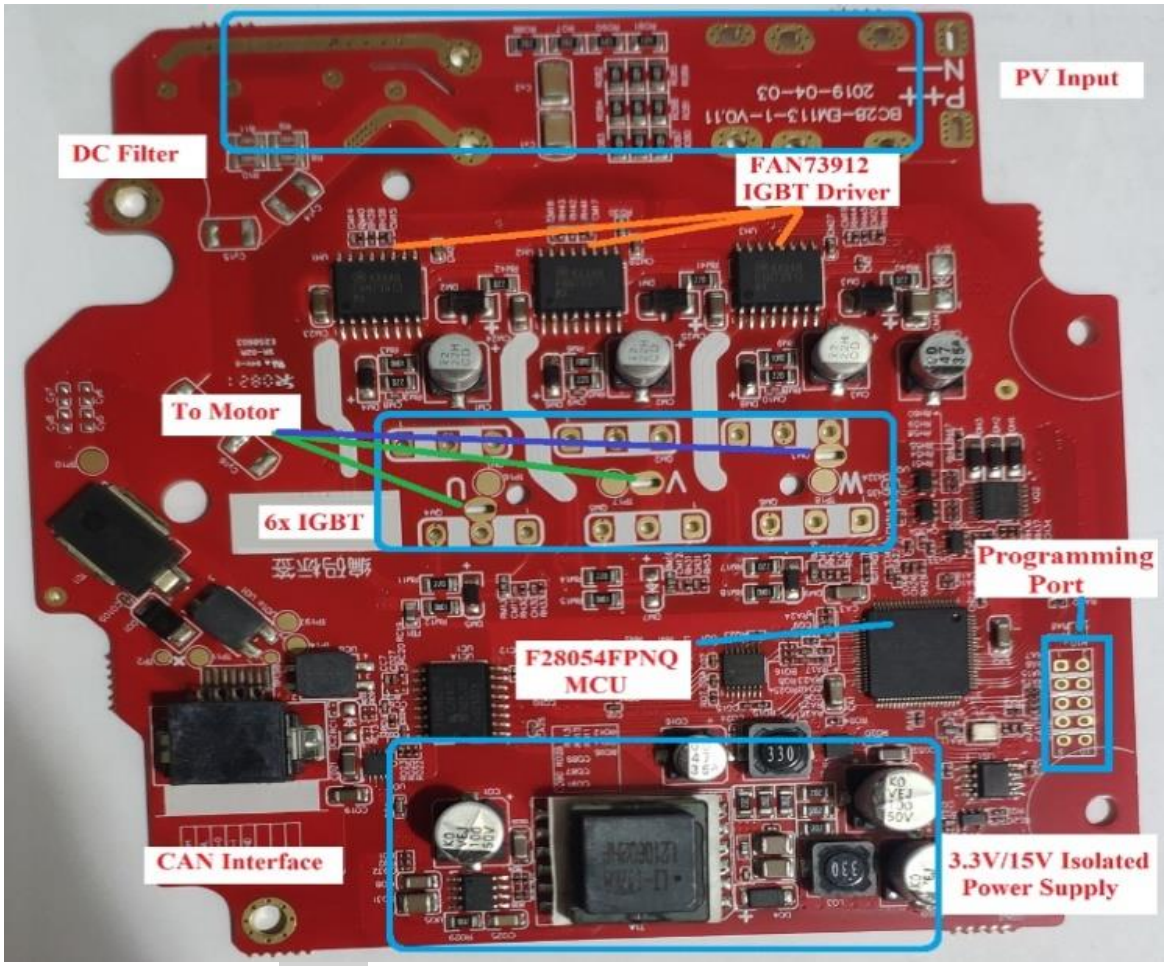

Fig. 18 The Developed ACIM Three-Phase Inverter.

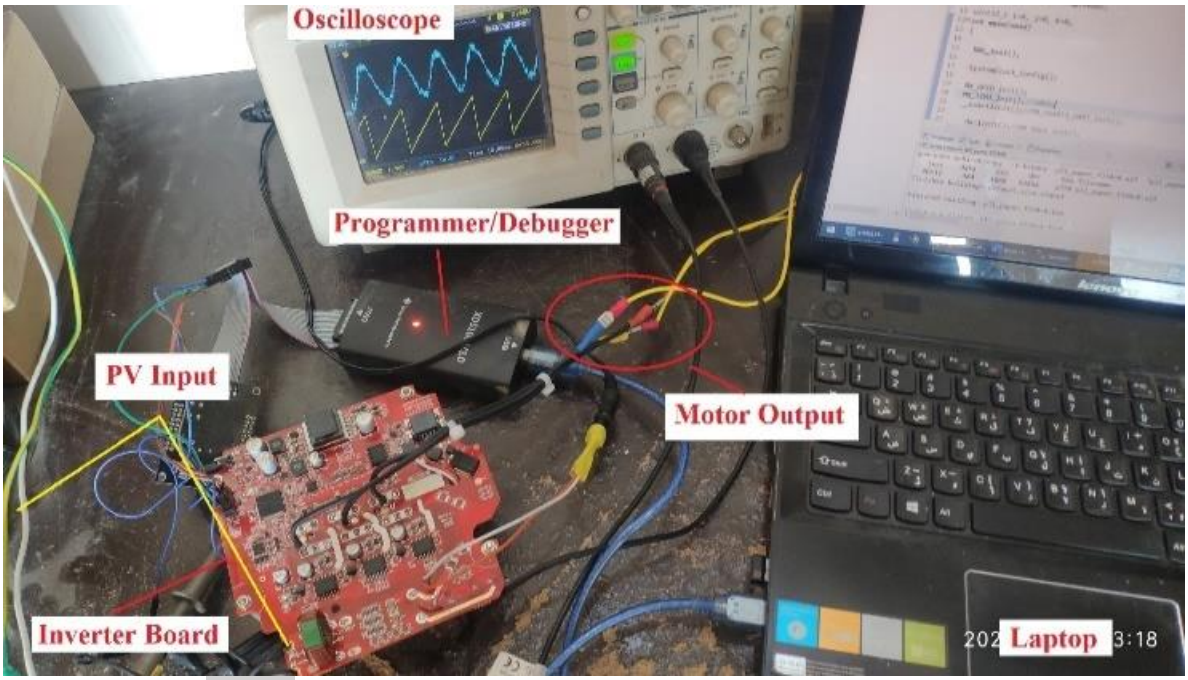

Fig. 19 Experimental in-the-Field Setup for the Designed System.

Fig. 20 The Installed PV Array (Top), Submersible ACIM Pump (Middle), and the Field to be Irrigated by the System (Bottom).

8.IN-FIELD RESULTS

a- FOC and Speed Estimator Results

After programming the DSP processor in the inverter board, the inverter was commanded to operate at specific speeds determined manually (not by the MPPT algorithm) to test the field control, flux, and speed estimation. At 700V open circuit voltage from the PV array, 2500 rpm (264 rad/s) was set as the reference speed for the motor. Fig. 21 shows the current waveform of phase A versus the estimated angle. The software variables, such as estimated speed, flux, and rotor angle, were visualized using the Digital to Analog Converter (DAC) in the DSP processor to be able to plot in the oscilloscope. The stationary reference frame components of the motor current (α, β) are shown in Fig. 22.

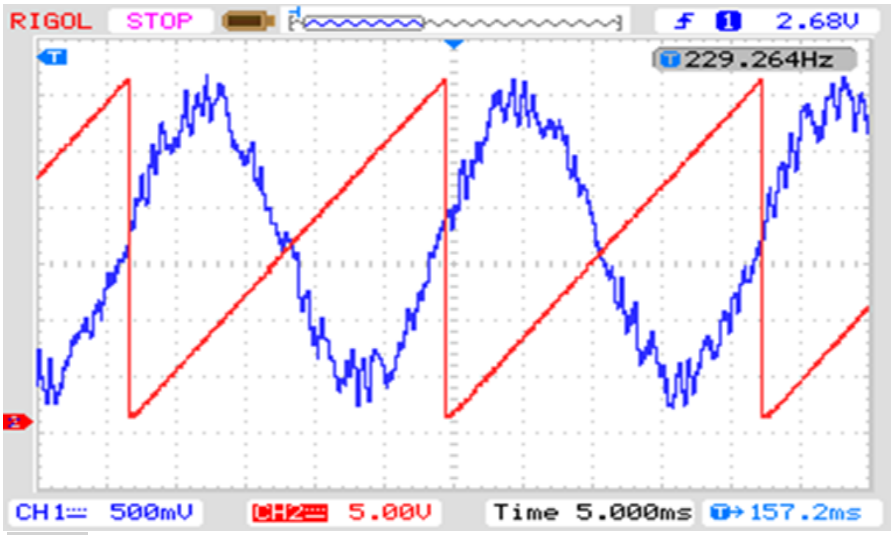

Fig.21 Phase A Current (Blue) Versus Estimated Angle (Red) at 2500 rpm.

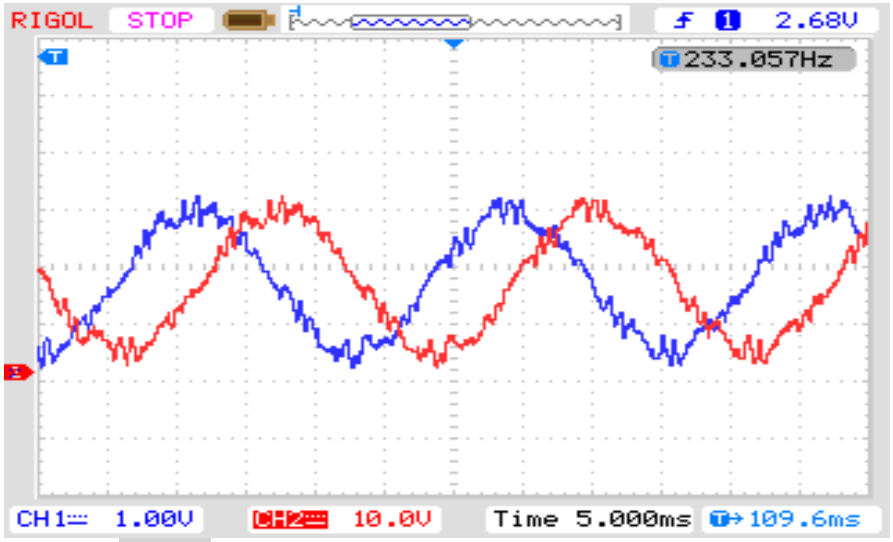

Fig. 22 (α, β) Components of Motor Current (10A/div).

The motor speed was suddenly changed from 2500 to 2400 rpm to mimic a falling step change for the speed controller behavior testing. The controller showed a slight undershoot of -12 rpm (0.5 %). The speed estimation was also recorded along with the actual speed (the real speed sensed using an attached encoder to the motor). The estimated speed had ±25 rpm minimum accuracy at the speed range of 1% at 2500 rpm and 0.83% at the nominal speed of the motor, as depicted in Fig.23.

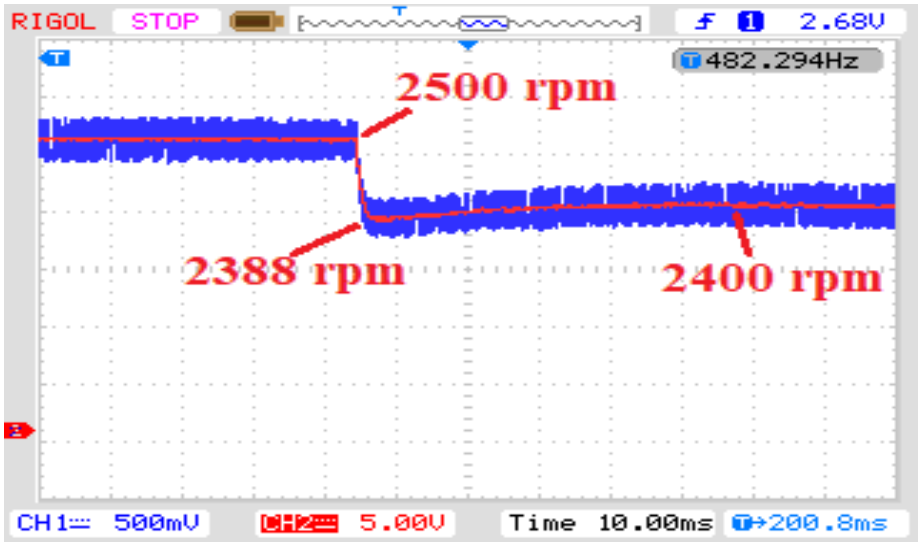

Fig. 23 Actual (Red) vs. Estimated (Blue) Speed for the Implemented System.

b- MPPT Controller Results

The MPPT controller of the system optimizes the motor's speed based on the PV array's available electricity, which guarantees the motor operation at its optimum speed when sufficient solar energy is available and regulates the speed when solar conditions are less favorable. This strategy maximizes the motor's utilization of the available solar energy. The system was tested under four insolation conditions on a sunny day at different hours. Table 1 shows the PV array voltage, current, and motor speed for various insolation conditions.

The MPPT efficiency is a factor in which the given conditions were simulated using MATLAB to obtain the theoretical MPP of the PV array and then compared to the actual values listed in Table 1. The irradiation was measured using a Fluke IRR1-SOL irradiance meter. As noted in Table 1, the insolation condition directly affected the motor speed and was decided by the MPPT controller to run the motor at the maximum possible speed.

Table 1 Designed System Key Specifications.

Irradiation (W/m²)	MPPT Eff. (%)	V_{PV} (V)	I_{PV} (A)	P_{PV} (W)	Motor Speed (rpm)
920	-	713	7.78	> 5500	2956
843	-	710	7.73	> 5500	2968
367	-	630	8.67	> 5500	2967
313	99.3	612	8.24	5043	2732
263	99.2	609	6.93	4220	2286
223	98.9	605	5.88	3652	1973
183	98.2	602	4.83	2905	1564
112	99.4	591	2.95	1745	967
88	99.1	586	2.31	1357	736
56	98.4	573	1.47	845	438

9.CONCLUSIONS

This research study presented thorough overview of the mandatory hardware and control features for Field-Oriented Control (FOC) in irrigation applications. Using a sensorless procedure for speed approximation in an ACIM demonstrated outstanding accuracy, with an inaccuracy ratio of smaller than 1 %. This scheme eradicates the requirement for pricey and burdensome speed sensors, backing to cost savings and system oversimplification. The notable behavior of the speed control, with a 2 ms response time and a -0.5% undershoot, revealed its precision in regulating motor speeds. This degree of control is crucial for uses agriculture applications in which satisfying particular motor speeds is critical for best features. In accumulation, the incorporation of a highest PowerPoint monitoring (MPPT) controller for precisely observing the utmost power output of a photovoltaic (PV) array expressively succeeded. The association between the realized MPPT controller and a simulation model under same conservational circumstances shown a substantial corresponding result, indicating the controller's reliability and stoutness. The blend of sensorless speed valuation, effective speed control, and accurate MPPT tracking made incredible outcomes in the irrigation organization. These outcomes backing boosted sustainability and cost investments and aggregate functioning efficiency. This study discoveries have the prospective to outgrowth improvements in irrigation expertise and the integration of sustainable energy, occasioning in significant benefits for agricultural throughput and ecological preservation.

APPENDIX

ACIM Parameters

5.5 kW, 3-phase, 400 V, 8 poles, Rs=0.303 Ω, Lls=0.00183 H, Rr=0.41 Ω, Llr=0.00183 H, Lm=0.03803 H.

REFERENCES

[1] Kant K, Jain C, Singh B. **A Hybrid Diesel-Wind PV-Based Energy Generation System with Brushless Generators**. *IEEE Transactions Industrial Informatics* 2017; **13**(4): 1714–1722.

[2] Deo S, ain CJ, Singh B. **A PLL-Less Scheme for Single-Phase Grid Interfaced Load Compensating Solar PV Generation System**. *IEEE Transactions Industrial Informatics* 2015; **11**(3): 692–699.

[3] Sashidhar S, Fernandes BG. **A Novel Ferrite SMDS Spoke-Type BLDC Motor for PV Bore-Well Submersible Water Pumps**. *IEEE Transactions on Industrial Electronics* Jan. 2017; **64**(1): 104–114.

[4] Carannante G, Fraddanno C, Pagano M, Piegari L. **Experimental Performance of MPPT Algorithm for Photovoltaic Sources Subject to Inhomogeneous Insolation**. *IEEE Transactions on Industrial Electronics* 2009; **56**(11): 4374-4380.

[5] Mahmmoud ON, Gaeid KS, Nashi AF, Siddiqui KM. **Induction Motor Speed Control with Solar Cell Using MPPT Algorithm by Incremental Conductance Method**. *Tikrit Journal of Engineering Sciences* 2020; **27**(3): 8-16.

[6] Cheles M. **Sensorless Field Oriented Control (FOC) of an AC Induction Motor (ACIM)**. Microchip Technology Inc.; 2008: 1-34.

[7] Li H, Curiac RS. **Designing More Efficient Large Industrial Induction Motors by Utilizing the Advantages of Adjustable-Speed Drives**. *IEEE Transactions Industrial Applications* 2010; **46**(5): 1805–1809.

[8] Marcetic P, Adzic EM. **Improved Three-Phase Current Reconstruction for Induction Motor Drives with DC-**

Link Shunt. *IEEE Transactions on Industrial Electronics* 2010; **57**(7): 2454–2462.

[9] Lee K, Yao W, Chen B, Lu Z, Yu A, Li D. **Stability Analysis and Mitigation of Oscillation in an Induction Machine**. *IEEE Transactions Industrial Applications* 2014; **50**(6): 3767–3776.

[10] Obeidi N, Kermadi M, Belmadani B, Allag A, Achour L, Mekhilef S. **A Current Sensorless Control of Buck-Boost Converter for Maximum Power Point Tracking in Photovoltaic Applications**. *Energies* 2022; **15**(20): 7811.

[11] Anwer AMO, Omar FA, Bakir H, Kulaksiz AA. **Sensorless Control of a PMSM Drive Using EKF for Wide Speed Range Supplied by MPPT Based Solar PV System**. *Elektronika ir elektrotechnika* 2020; **26**(1): 32-39..

[12] Ranjith S, Abeykoon C, Maithripala D. **Design of a Sensorless Field Oriented Control Drive for Brushless DC Motors.** *In: Proceedings of the 9th International Conference of Control, Dynamic Systems, and Robotics (CDSR'22)* 2022 Jun. 02-04; Niagara Falls, Canada: Paper No. 180.

[13] Van Bavo. **Practical Ferrioxalate Actinometry for the Determination of Photon Fluxes in Production-Oriented Photoflow Reactors**. *Organic Process Research & Development* 2022; **26**(8): 2392-2402.

[14] De Brito, Moacyr AG. **Current Sensorless Based on PI MPPT Algorithms**. *Sensors* 2023; **23**(10): 4587, (1-17).

[15] Ali Z, Abbas SZ, Mahmood A, Ali SW, Javed SB, Su CL. **A Study of a Generalized Photovoltaic System with MPPT Using Perturb and Observer Algorithms under Varying Conditions**. *Energies* 2023; **16**(9): 3638, (1-21).

[16] Kumar R, Singh B. **Solar Pv Powered BLDC Motor Drive for Water Pumping Using Cuk Converter**. *IET Electric Power Applications* 2017; **11**(2): 222-232.

[17] Kumar R, Singh B. **BLDC Motor Driven Solar PV Array Fed Water Pumping System Employing Zeta Converter**. *IEEE 6th India International Conference on Power Electronics (IICPE)* 2014 December 8-10; Kurukshetra, India: 213-218.

[18] Narendra A, Panda VNA, Tiwary N, Kumar A. **A Single-Stage SPV-FED Reduced Switching Inverter-based Sensorless Speed Control of IM for Water Pumping Applications**. *International Transactions on Electrical Energy Systems* 2022; **2022**: 3805791, (1-12).

[19] Hassan Q. **Solar Powered Water Pumping System for a Rural Village**. *Ecological Engineering & Environmental Technology* 2023; **24**(2): 214-223.

[20] Hmidet A, Subramaniam U, Elavarasan RM, Raju K, Diaz M, Das N, Boubaker O. **Design of Efficient Off-grid Solar Photovoltaic Water Pumping System Based on Improved Fractional Open Circuit Voltage Mppt Technique**. *International Journal of Photoenergy* 2021; **2021**: 4925433, (1-18).

[21] Lalithasymala A, Ravi Kishore D. **Comparative Analysis on VSI and CSI Based Solar Photovoltaic Source FED BLDC Motor Drive with Boost Converter for Water Pumping System**. *International Journal for Modern Trends in Science and Technology* 2021; **7**(3): 62-70.

[22] Singh B, Kumar R. **Simple Brushless DC Motor Drive for Solar Photovoltaic Array Fed Water Pumping System**. *IET Power Electronics* 2016; **9**(7): 1487-1495.

[23] Sinaga R. **Design and Construction of a Portable Solar Water Pump 3000 Litter Per Hour**. *In Proceedings of the 4th International Conference on Applied Science and Technology on Engineering Science (iCAST-ES 2021)* 2021; Indonesian Polytechnics Consortium: 1210-1216.

[24] Samikannu R, Krishnamoorthy V, Chinnaraj G, Mani G. **Fuzzy Logic Control for Solar PV FED Modular Multilevel Inverter Towards Marine Water Pumping Applications**. *IEEE Access* 2021; **9**: 88524-88534.

[25] Vamja R, Mulla M. **Multipurpose Battery-Assisted Solar Water Pumping System for Off-grid Applications: Design and Development**. *IET Electric Power Applications* 2020; **14**(14): 2717-2730.

[26] Kumar R, Singh B. **BLDC Motor Driven Solar PV Array Fed Water Pumping System Employing Zeta Converter**. *IEEE 6th India International Conference on Power Electronics (IICPE)* 2014 December 8-10; Kurukshetra, India: 1-6.

[27] Velkov T, Chingoski V. **Speed Control of AC Motors for Electric Vehicles Using Field Oriented Control**. *Balkan Journal of Applied Mathematics and Informatics* 2023; **6**(1): 37-48.

[28] Zeddini MA, Krim S, Mimouni MF. **Experimental Validation of an Advanced Metaheuristic Algorithm for Maximum Power Point Tracking of a Shaded Photovoltaic System: A Comparative Study Between Three Approaches**. *Energy Reports* 2023; **10**: 161-185.

[29] Ba OA, Ndiaye A, Ba A, Tankari MA. **Optimization of the P&O-MPPT controller by the adaptive method (Ad-P&O) for stand-alone PV systems**. *In 2023 11th International Conference on Smart Grid (icSmartGrid)* 2023 June 4-7; France Paris: 1-8.